Efficient Modeling of Power/Ground Planes Using Delay-Extraction-Based Transmission Lines

Sourajeet Roy, *Student Member, IEEE*, Anestis Dounavis, *Member, IEEE*

***Abstract*— This paper presents an efficient approach for modeling irregular shaped power distribution networks (PDN) in high-speed packages. The proposed methodology is based on discretization of the plane into an orthogonal grid of transmission line segments. Using a delay-extraction-based model for each line segment, a compact circuit model is achieved where the size of the circuit matrices depend only on the nodes of the orthogonally discretized structure and all other internal nodes due to the macromodel are eliminated. This approach of eliminating the internal variable due to the transmission line macromodel is further extended to model skin effect losses without augmenting the circuit matrices. The proposed work has been successfully implemented for a variety of PDN structures and geometries and has been shown to yield significant savings in memory and run time costs compared to the existing simulation program with integrated circuits emphasis macromodels.**

***Index Terms*— Delay extraction, macromodeling, networks, power distribution, resonance, skin effect, transmission lines.**

I. Introduction

POWER distribution networks (PDNs) provide a path for the power supply to the core logic circuits and I/O drivers of high-speed digital systems [1]. Ideally, a PDN should exhibit low impedance over a large frequency range of operation so that the transient currents induced by the simultaneous switching of digital circuits does not lead to excessive noise propagation over the PDN [1]–[8]. However, with the progressive increase in clock speed, scaling of supply voltage, high switching speed of logic circuits, and reduced noise margins, effects like ground bounce, electromagnetic (EM) interference, and delta-I noise arising in the PDNs can quickly lead to undesirable voltage fluctuations and propagation delays in the chip, board, and packaging levels [1]–[8]. Hence PDNs are fast emerging as a critical area for electromagnetic compatibility and signal integrity verification for high-speed packages.

Traditionally, the electric performance of PDNs was studied using numerical techniques such as finite difference time domain [9]–[10], method of moments [11], finite element method [12] and partial element equivalent circuit [13], to name a few. While such full-wave techniques provide a high degree of versatility and accuracy, they result in large systems of equations which may be computationally prohibitive for efficient noise predictions, especially when the PDNs are terminated with nonlinear circuits [14].

An alternative approach to modeling PDNs is based on deriving equivalent circuit models that match the frequency response of the structure within a prescribed bandwidth [4]–[8], [14]–[21]. These equivalent circuit models are easily realizable in simulation program with integrated circuits emphasis (SPICE) and can be linked to nonlinear terminations using ports. Some of the earliest SPICE models relied on importing *S*-parameter data [6] and the resonator model [15]. More popular models are based on discretization of the plane into a grid of transmission lines [4]–[7], [16]–[21], since they can be easily extended to irregular plane structures. One approach toward modeling the transmission line segments is using conventional lumped resistance-inductance-conductance-capacitance (RLGC) elements [7], [16]–[19]. However, the accuracy of PDN models using lumped elements is limited to scenarios where the rise time of the excitation is much higher than the propagation time over the planes [6]. As the frequency of operation increases, larger number of lumped sections have to be included, leading to larger circuit matrices. Moreover, to model high-frequency effects like skin effect in SPICE requires additional lumped elements (e.g., *RL* ladder networks [22]), which can quickly lead to prohibitively large memory and run time costs. An alternative method to model transmission lines is based on HSPICEs W-element [21], [23]. The W-element model uses delay extraction similar to method of characteristics algorithms [24]–[28] and is very efficient in modeling long low-loss transmission lines [such as printed circuit board (PCB) interconnects] when compared to the conventional lumped model which requires many sections [29]. However, the discretization of a PDN structure leads to many electrically short transmission line segments. As a result, the efficiency of the W-element over lumped models for long transmission lines is not transferable to the example of PDN. Other alternative techniques to model transmission lines have also been proposed [5], [30]–[33], which can be used to model PDNs. However, all the above SPICE models may still lead to large circuit matrices due to the introduction of internal nodes in representing each transmission line segment in the modified nodal analysis (MNA) formulation used by SPICE. Other techniques to improve the memory and central processing unit (CPU)

Manuscript received August 10, 2010; revised January 26, 2011; accepted February 6, 2011. Date of publication April 21, 2011; date of current version June 2, 2011. This work was supported in part by the Natural Sciences and Engineering Research Council of Canada, Canada Foundation for Innovation, Canadian Microelectronics Corporation, and the Ministry of Research and Innovation-Early Research Award. Recommended for publication by Associate Editor J. Tan upon evaluation of reviewers' comments.

The authors are with the Department of Electrical and Computer Engineering, University of Western Ontario, London, ON N6A 5B9, Canada (email: sroy33@uwo.ca, adounavis@eng,uwo.ca).

Color versions of one or more of the figures in this paper are available online at http://ieeexplore.ieee.org.

Digital Object Identifier 10.1109/TCPMT.2011.2117423

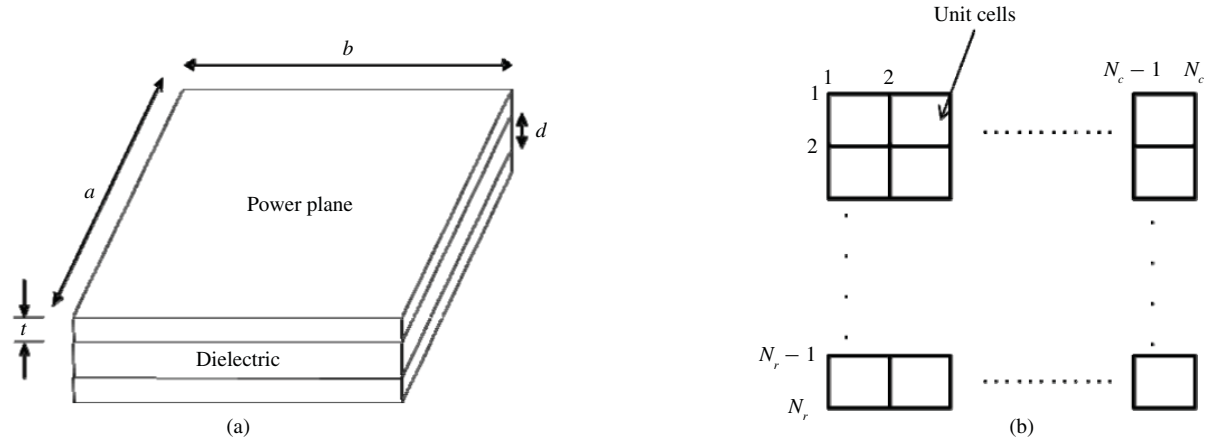

Fig. 1. Modeling of PDN based on discretization of the structure into unit cells. (a) Rectangular PDN structure. (b) Discretization of structure into unit cells.

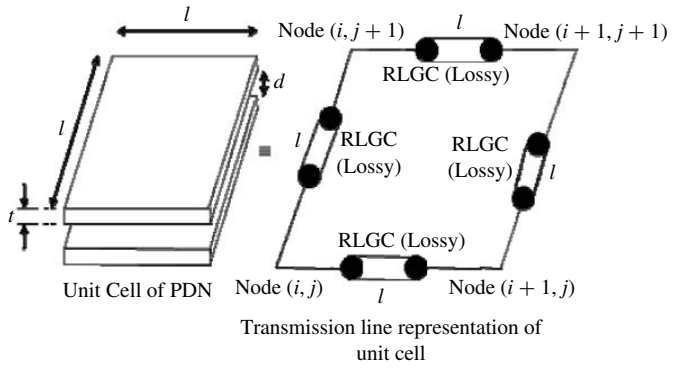

Fig. 2. Modeling of unit cell of PDN using grid of transmission lines.

costs in simulating PDN in SPICE are based on model order reduction [18], [19].

This paper presents an efficient broadband PDN model. The proposed model exploits the segmentation methodology of the delay extraction-based macromodeling algorithm (DEPACT) macromodel [34]–[36] to model the short transmission line segments of the PDN. The resulting circuit equations are compressed by eliminating all the nodes internal to each transmission line segment created by the DEPACT macromodel. As a result, the number of equations depends only on the number of nodes of the orthogonally discretized structure. This methodology to eliminate internal variables due to the transmission line macromodel is also extended to model skin effect losses without augmenting the original circuit matrices. This leads to significant savings in memory and run time costs when compared to traditional SPICE models. The proposed algorithm leads to a compact set of delay algebraic linear equations to efficiently model PDNs.

II. Review of PDN Modeling and DEPACT Macromodel

In order to better explain the proposed model, this section briefly reviews the traditional modeling methodology of PDNs using transmission line segments followed by a review of the DEPACT macromodel.

A. Modeling of the PDN

A PDN consisting of a rectangular signal/ground plane with single layered dielectric in between and assumed to be free of any surface irregularity is considered in Fig. 1(a). The plane can be discretized into numerous rectangular unit cells shown in Fig. 1(b). The equivalent circuit representing a unit cell can be obtained from the physical and electrical parameters of the plane using a quasi-static model, provided the dielectric separation between the power and ground plane pairs is much smaller compared to the dimensions of the plane [7]. Considering a square unit cell of dimensions (l) with a dielectric separation of (d) between planes, thickness of metal (t), metal conductivity (σ), loss tangent (δ) and relative permittivity (ε_r), the equivalent electrical parameters are

$$R = \frac{2}{\sigma t}, \quad C = \varepsilon_o \varepsilon_r \frac{l^2}{d}, \quad L = \mu_o d,$$
$$G = \omega C \tan(\delta), \quad R_s = 2\sqrt{\frac{s\mu_0}{\sigma}} \tag{1}$$

where $s = j2\pi f$, f is the instantaneous frequency, ε_o and μ_o are the permittivity and the permeability of free space, ε_r is the relative permittivity of the dielectric and R, L, C, G, and R_s are the resistive, inductive, capacitive, conductive, and skin effect losses contribution of the unit cell, respectively [7]. Each cell can be represented by a grid of four transmission line segments, as shown in Fig. 2, with each segment having the per-unit-length (p.u.l.) resistive, capacitive, inductive, conductive, and skin effect loss parameters of

$$R_i = \frac{2R}{l}, \quad C_i = \frac{C}{4l}, \quad L_i = \frac{2L}{l},$$
$$G_i = \frac{G}{4l}, \quad R_{si} = 2\frac{R_s}{l} \tag{2}$$

respectively, when the line segment is located at the edge of the structure and

$$R_i = \frac{R}{l}, \quad C_i = \frac{C}{2l}, \quad L_i = \frac{L}{l},$$
$$G_i = \frac{G}{2l}, \quad R_{si} = \frac{R_s}{l} \tag{3}$$

respectively, when the line segment is located inside the grid. Hence the above discretization of PDN results in N_r rows and

N_c columns of line segments with a total of $(N_c-1)*N_r+(N_r-1)*N_c$ transmission lines and $(N_c-1)*(N_r-1)$ unit cells [Fig. 1(b)]. Combining the transmission line segments representing each unit cell with p.u.l. parameters of (2) and (3), the distributed PDN can be represented by a grid of orthogonal transmission line elements as described in [4]–[7].

The next section briefly reviews the DEPACT algorithm which will be used to model each transmission line segment.

B. Overview of DEPACT Model

Coplanar transmission lines are described by the Telegraphers equations [37]. The solution of Telegraphers equations for a two-conductor transmission line can be written as an exponential matrix function [37] as

$$\begin{bmatrix} V(l,s) \\ -I(l,s) \end{bmatrix} = e^{\boldsymbol{\Phi}} \begin{bmatrix} V(0,s) \\ I(0,s) \end{bmatrix} \tag{4}$$

where

$$\boldsymbol{\Phi} = \boldsymbol{A} + s\boldsymbol{B}; \quad \boldsymbol{A} = \begin{bmatrix} 0 & -(R_i+R_{si})l \\ -G_i l & 0 \end{bmatrix}; \quad \boldsymbol{B} = \begin{bmatrix} 0 & -L_i l \\ -C_i l & 0 \end{bmatrix} \tag{5}$$

with V and I representing the terminal voltage and current variables of the transmission line, respectively, and l the length of the transmission line.

The basic idea of the DEPACT algorithm is to separate the delay terms ($e^{s\boldsymbol{B}}$) from $e^{(\boldsymbol{A}+s\boldsymbol{B})}$. However, this is not a trivial task since the matrices $\boldsymbol{A}$ and s$\boldsymbol{B}$ do not commute, (i.e., $e^{(\boldsymbol{A}+s\boldsymbol{B})} \neq e^{\boldsymbol{A}}e^{s\boldsymbol{B}}$). To approximate $e^{(\boldsymbol{A}+s\boldsymbol{B})}$ in terms of a product of exponentials, a modified Lie product [35] is used as

$$e^{\boldsymbol{A}+s\boldsymbol{B}} \approx \prod_{i=1}^{n} \boldsymbol{\Psi}_i + \varepsilon_n \text{ and } \boldsymbol{\Psi}_i = e^{\frac{\boldsymbol{A}}{2n}} e^{\frac{s\boldsymbol{B}}{n}} e^{\frac{\boldsymbol{A}}{2n}} \tag{6}$$

where n is the number of sections. The associated error of the approximation scale to the second power of the number of sections n, as $||\varepsilon_n|| \cong O(1/n^2)$ [35], i.e., (6) quickly converges to the exponential matrix of (4) with increase of number of sections, n. Equation (6) shows that the exponential function of (4) can be divided into subsections of $e^{\boldsymbol{A}/2n}$ and $e^{s\boldsymbol{B}/n}$. The matrix $e^{s\boldsymbol{B}/n}$ represents a lossless transmission line sections, which can be expressed in the time domain as delay algebraic equations [35], [37] and $e^{\boldsymbol{A}/2n}$ represents the attenuation matrix which can be modeled using lumped circuit elements [35], [36].

It is worth noting that the application of any SPICE model to PDN structures leads to the formulation of a linear circuit matrix equation in the frequency domain of the form $\boldsymbol{Ax} = \boldsymbol{B}$, where $\boldsymbol{A}$ represents the MNA matrix of the equivalent SPICE network of the PDN, $\boldsymbol{B}$ is the vector of sources and $\boldsymbol{x}$ represents the vector of unknown current and voltage variables of the discretized structure. Irrespective of the SPICE model used, there are two major factors contributing to the size of the $\boldsymbol{A}$ matrix. One factor is the number of nodes created because of the discretization of the PDN structure into an orthogonal grid of transmission line segments to match the response up to a maximum frequency of interest. Another factor is the introduction of additional internal nodes due to the macromodel used to model each transmission line segment in the MNA formulation. In this paper, the DEPACT macromodel is used to efficiently represent the transmission lines of the discretized PDN [34]–[36]. The resulting circuit equations are written in such a way that all internal nodes due to the transmission line macromodel are eliminated, thereby reducing the computational burden of the proposed model. This will be discussed in more detail in the following section.

III. Development of Proposed Model

The development of the proposed algorithm begins with transmission line segments with frequency-independent parameters and is extended to deal with transmission line segments with skin effect losses.

A. Modeling PDN with Frequency Independent p.u.l. Parameters

To develop the proposed methodology, consider a transmission line segment between nodes (p,q) and $(p+1,q)$ from among the grid of transmission lines as shown in Fig. 2. The p.u.l. parameters of the line segment are frequency independent and are given by (2) and (3) (with $R_{si}=0$ and all other p.u.l. parameters are constant, not necessarily zero). Applying (6) on the line segment with $n=1$, the terminal voltage–current at both near and far ends can be expressed as

$$\begin{bmatrix} V_{p+1,q} \\ -I_{p+1,q} \end{bmatrix} = e^{\frac{\boldsymbol{A}}{2}} e^{s\boldsymbol{B}} e^{\frac{\boldsymbol{A}}{2}} \begin{bmatrix} V_{p,q} \\ I_{p,q} \end{bmatrix} \tag{7}$$

where $V_{p,q}$, $V_{p+1,q}$, $I_{p,q}$, $I_{p+1,q}$ are the terminal voltages and current variables of the line segment. In this formulation, it is assumed that the discretization of PDN leads to many short transmission line segments, which can be modeled using one DEPACT segment [34]. However, if additional segments are required, the procedure of this section can easily be extended to accommodate $n>1$ in (7). The lossy and lossless sections of (7) can be expressed as

$$e^{\frac{\boldsymbol{A}}{2}} = \begin{bmatrix} A_i & B_i \\ C_i & D_i \end{bmatrix} = \begin{bmatrix} \cosh\left(\frac{lw_0}{2}\right) & -\frac{1}{g_0}\sinh\left(\frac{lw_0}{2}\right) \\ -g_0\sinh\left(\frac{lw_0}{2}\right) & \cosh\left(\frac{lw_0}{2}\right) \end{bmatrix} \tag{8}$$

$$e^{s\boldsymbol{B}} = \begin{bmatrix} \hat{A}_i & \hat{B}_i \\ \hat{C}_i & \hat{D}_i \end{bmatrix} = \begin{bmatrix} \cosh(sl\gamma_i) & -Z_0\sinh(sl\gamma_i) \\ -\frac{1}{Z_0}\sinh(sl\gamma_i) & \cosh(sl\gamma_i) \end{bmatrix} \tag{9}$$

where $w_0=\sqrt{R_iG_i}$ $g_0=\sqrt{G_i/R_i}$, $\gamma_i=\sqrt{L_iC_i}$, and $Z_0=\sqrt{L_i/C_i}$. Note that when considering frequency-independent p.u.l. parameters, $e^{\boldsymbol{A}/2}$ is a constant matrix, while $e^{s\boldsymbol{B}/n}$ is always a function of frequency. Substituting $\cosh(sl\gamma_i)=(e^{sl\gamma_i}+e^{-sl\gamma_i})/2$ and $\sinh(sl\gamma_i)=(e^{sl\gamma_i}-e^{-sl\gamma_i})/2$ into (9) and using (8) and (9) in (7), the terminal voltage–current relationship of the line segment can be expressed as

$$\begin{aligned} &(A_i(1+e^{-2sl\gamma_i})-Z_0C_i(1-e^{-2sl\gamma_i}))V_{i,j} \\ &\quad +(B_i(1+e^{-2sl\gamma_i})-Z_0D_i(1-e^{-2sl\gamma_i}))I_{i,j} \\ &\quad -2e^{-sl\gamma_i}(A_iV_{i+1,j}+B_iI_{i+1,j})=0 \\ &(A_i(1+e^{-2sl\gamma_i})-Z_0C_i(1-e^{-2sl\gamma_i}))V_{i+1,j} \\ &\quad +(B_i(1+e^{-2sl\gamma_i})-Z_0D_i(1-e^{-2sl\gamma_i}))I_{i+1,j} \\ &\quad -2e^{-sl\gamma_i}(A_iV_{i,j}+B_iI_{i,j})=0. \end{aligned} \tag{10}$$

It is observed that (10) has two terminal voltage and two terminal current variables with only two equations describing them. The remaining two equations are obtained from the Kirchhoff's current law (KCL) equation where the sum of currents entering nodes (p, q) and $(p+1, q)$ from the surrounding line segments equal to zero. Assembling (10) for each transmission line segment and the KCL equations for each node of the discretized PDN, the circuit matrix to model the entire PDN can be expressed as

$$\left(\boldsymbol{A}_T + \sum_{i=1}^{N} e^{-s\gamma_i l}\boldsymbol{B}_T^{(i)} + \sum_{i=1}^{N} e^{-2s\gamma_i l}\boldsymbol{C}_T^{(i)}\right)\boldsymbol{X}(s) = \boldsymbol{P}\boldsymbol{u}(s) \tag{11}$$

where $\boldsymbol{A}_T, \boldsymbol{B}_T^{(i)}, \boldsymbol{C}_T^{(i)}$ are the constant coefficient matrices, $\boldsymbol{X}(s)$ is the vector containing the unknown nodal voltages, terminal currents of each line segment, and the input/output port currents; and N is the number of different delays $(\gamma_i l)$ when an irregular discretization is used or p.u.l. parameters vary due to different materials used over the PDN geometry. Equation (11) can be converted into time domain for transient analysis and is described as

$$\boldsymbol{A}_T\boldsymbol{X}(t) + \sum_{i=1}^{N}\boldsymbol{B}_T^{(i)}\boldsymbol{X}(t-\gamma_i l) + \sum_{i=1}^{N}\boldsymbol{C}_T^{(i)}\boldsymbol{X}(t-2\gamma_i l) = \boldsymbol{P}\boldsymbol{u}(t). \tag{12}$$

In the following section, the proposed methodology is extended for PDN with frequency dependent p.u.l. parameters.

B. Proposed Macromodel for Frequency-Dependent Parameters

With the signal switching speed increasing beyond the gigahertz range, PDN macromodels must include high-frequency effects such as the skin effect for greater accuracy. In the proposed model, the skin effect resistance is assumed to be dependent on the square root of frequency as $\sqrt{s}$ [7]. To incorporate the skin effect in (7), the $\sqrt{s}$ dependency of $R_{si}(s)$ in (1) is approximated as a rational approximation, similar to [38] scaled by the properties of the material as

$$R_{si}(s) = 2\sqrt{\frac{\mu_0}{\sigma}}\sqrt{s} \approx 2\sqrt{\frac{\mu_0}{\sigma}}\left(r_{i0} + \sum_{j=1}^{N_p}\frac{r_{ij}}{s-p_{ij}}\right) \tag{13}$$

where r_{i0} is the constant, r_{ij} and p_{ij} are the residues and poles, respectively, of the rational approximation of $\sqrt{s}$; and N_p is the order of the approximation. The order of the approximation (N_p) is chosen such that the root mean square (RMS) error of the approximation of (13) over the entire bandwidth of operation $(0–F_{\max})$ is within a prescribed tolerance. Note that the rational approximation of $\sqrt{s}$ is independent of the physical and electrical parameters of the PDN as well as the discretization used. As a result, the function $\sqrt{s}$ can be approximated offline for various orders of accuracy while ensuring that the rational approximation is positive real to maintain the passivity of the macromodel. Ensuring the passivity of the macromodel is important since non-passive but stable macromodels when connected to arbitrary circuit elements can lead to unstable systems [39]. Equation (13) is a valid assumption for high frequencies when the skin effect is significant. However, for low-frequency operation, when including edge and proximity effects, $R_{si}(s)$ can be represented as tabulated data obtained from electromagnetic simulations or measurements. In any case, the $R_{si}(s)$ parameter can thereafter be approximated using rational functions. To include the skin effect losses of (13), the lossy segment of the model in (8) is rewritten as

$$e^{\frac{\boldsymbol{A}(s)}{2}} = e^{\begin{bmatrix} 0 & -(R_i+R_{si})l/2 \\ -G_i l/2 & 0 \end{bmatrix}} = \begin{bmatrix} A_i(s) & B_i(s) \\ C_i(s) & D_i(s) \end{bmatrix} \tag{14}$$

where the entries $A_i(s), B_i(s), C_i(s)$, and $D_i(s)$ are now frequency dependent due to the skin effect losses. To determine the time domain representation of $A_i(s), B_i(s), C_i(s)$, and $D_i(s)$, the exponential matrix of (14) is approximated using a closed-form Padé expression [30]. Since the delays of the transmission line segment are already extracted in e^{sB} matrix of (7), a Padé order of 1/1 (i.e., $e^x = (1-x/2)^{-1}(1+x/2)$) is sufficient to accurately approximate (14) as

$$e^{\frac{\boldsymbol{A}(s)}{2}} \approx \left[\boldsymbol{I} - \frac{\boldsymbol{A}(s)}{4}\right]^{-1}\left[\boldsymbol{I} + \frac{\boldsymbol{A}(s)}{4}\right]. \tag{15}$$

Substituting the rational approximation of (13) and (15) in (14), the $A_i(s), B_i(s), C_i(s)$, and $D_i(s)$ of (14) can now be written in rational form as

$$\begin{aligned} A_i(s) = D_i(s) &\approx a_{i0} + \sum_{j=1}^{N_p}\frac{a_{ij}}{s-\tilde{p}_{ij}} \\ B_i(s) &\approx b_{i0} + \sum_{j=1}^{N_p}\frac{b_{ij}}{s-\tilde{p}_{ij}} \\ C_i(s) &\approx c_{i0} + \sum_{j=1}^{N_p}\frac{c_{ij}}{s-\tilde{p}_{ij}} \end{aligned} \tag{16}$$

where a_{ij}, b_{ij}, c_{ij}, and $\tilde{p}_{ij}$ are obtained by substituting (13) and (14) in (15). Next, substituting $\cosh(sl\gamma_i) = (e^{sl\gamma_i} + e^{-sl\gamma_i})/2$ and $\sinh(sl\gamma_i) = (e^{sl\gamma_i} - e^{-sl\gamma_i})/2$ into (9) and using (16) and (9) in (7) yields a terminal voltage–current relationship similar to (10), as

$$\begin{aligned} &(A_i(s)(1+e^{-2s\gamma_i l}) - Z_0C_i(s)(1-e^{-2s\gamma_i l}))V_{p,q} \\ &\quad +(B_i(s)(1+e^{-2s\gamma_i l}) - Z_0D_i(s)(1-e^{-2s\gamma_i l}))I_{p,q} \\ &\quad -2e^{-s\gamma_i l}(A_i(s)V_{p+1,q} + B_i(s)I_{p+1,q}) = 0 \\ &(A_i(s)(1+e^{-2s\gamma_i l}) - Z_0C_i(s)(1-e^{-2s\gamma_i l}))V_{p+1,q} \\ &\quad +(B_i(s)(1+e^{-2s\gamma_i l}) - Z_0D_i(s)(1-e^{-2s\gamma_i l}))I_{p+1,q} \\ &\quad -2e^{-s\gamma_i l}(A_i(s)V_{p,q} + B_i(s)I_{p,q}) = 0. \end{aligned} \tag{17}$$

As before, assembling (17) for each transmission line segment and the KCL equations for each node of the discretized PDN, the circuit matrix to model the entire PDN can be expressed in a compact form as

$$\sum_{i=1}^{N}\left(\tilde{\boldsymbol{A}}_T^{(i)}(s) + e^{-s\gamma_i l}\tilde{\boldsymbol{B}}_T^{(i)}(s) + e^{-2s\gamma_i l}\tilde{\boldsymbol{C}}_T^{(i)}(s)\right)\boldsymbol{X}(s) = \boldsymbol{P}\boldsymbol{u}(s) \tag{18}$$

where $\tilde{\boldsymbol{A}}_T$, $\tilde{\boldsymbol{B}}_T^{(i)}$, $\tilde{\boldsymbol{C}}_T^{(i)}$ are the matrices resulting from using (16) in (17), written in rational form as

$$\tilde{\boldsymbol{A}}_T^{(i)}(s) = \boldsymbol{A}_0^{(i)} + \sum_{j=1}^{N_p} \frac{\boldsymbol{A}_{ij}}{s - \tilde{p}_{ij}}$$
$$\tilde{\boldsymbol{B}}_T^{(i)}(s) \approx \boldsymbol{B}_0^{(i)} + \sum_{j=1}^{N_p} \frac{\boldsymbol{B}_{ij}}{s - \tilde{p}_{ij}}$$
$$\tilde{\boldsymbol{C}}_T^{(i)}(s) \approx \boldsymbol{C}_0^{(i)} + \sum_{j=1}^{N_p} \frac{\boldsymbol{C}_{ij}}{s - \tilde{p}_{ij}}. \tag{19}$$

The time domain solution of (19) is described as

$$\sum_{i=1}^{N} \Bigg[\boldsymbol{A}_0^{(i)} \boldsymbol{X}(t) + \boldsymbol{B}_0^{(i)} \boldsymbol{X}(t - \gamma_i l) + \boldsymbol{C}_0^{(i)} \boldsymbol{X}(t - 2\gamma_i l) + \sum_{j=1}^{N_p} \boldsymbol{A}_{ij} \int_0^t e^{\tilde{p}_{ij}(t-\tau)} \boldsymbol{X}(\tau) + \sum_{j=1}^{N_p} \boldsymbol{B}_{ij} \int_0^{t-\gamma_i l} e^{\tilde{p}_{ij}(t-\tau)} \boldsymbol{X}(\tau) d\tau + \sum_{j=1}^{N_p} \boldsymbol{C}_{ij} \int_0^{t-2\gamma_i l} e^{\tilde{p}_{ij}(t-\tau)} \boldsymbol{X}(\tau) d\tau \Bigg] = \boldsymbol{P}\boldsymbol{u}(t). \tag{20}$$

The terms under the integral in (20) represent the convolution terms of the rational approximation with the vector $X(t)$, which can be solved efficiently using a recursive convolution formulation [40] and has linear time complexity of $O(N_{time})$ [41], where N_{time} represents the number of time points of simulation.

Note that the formulation of the transmission line equations of (10) and (17) differs from that in [35]. The DEPACT macromodel of [35] uses the MNA stamps of a lossless transmission line and lumped resistive elements which leads to six equations for each line segment for the frequency-independent parameter case [35]. To include skin effect losses, an *RL* ladder is used which further increases the number of equations of each line segment [35]. Hence, using DEPACT macromodel in a MNA formulation requires $N_d = (8m + 13)\ N_c N_r - (4m + 6)(N_c + N_r) + N_o$ equations for the transient analysis of a PDN structure, where m is the number of sections of the *RL* ladder used to model the skin effect losses and N_o is the total number of ports of the structure. In comparison, the proposed methodology represents each transmission line using only the terminal voltage and current variables and eliminates all internal variables arising from the macromodel of the transmission line, thereby leading to a more compact model. For both frequency-independent and dependent parameter cases, the size of the circuit matrices of (12) and (20) is the same and equal to $N_t = 5N_c N_r - 2(N_c + N_r) + N_o$ because of the $2N_c(N_r - 1) + 2N_r(N_c - 1)$ equations to represent each transmission line segment using (10), (17), and $N_c N_r$ KCL equations for each node. Numerical examples of Section IV illustrate that the proposed model provides a significant reduction in memory and run time costs when compared with existing SPICE models.

C. Including Decoupling Capacitors

Decoupling capacitors are placed at strategic position of the PDN to provide a low-impedance path for the noise signal to the ground. They are commonly modeled as lumped *RLC* elements in series to represent the series equivalent resistive and inductive contribution of the capacitor along with the capacitance [7]. Since decoupling capacitors significantly change the impedance to the simultaneous switching noise (SSN) signal on the PDN, its effect must be included in the model.

Considering a single decoupling capacitor placed at the node (i, j), the additional circuit equations due to the decoupling capacitor are described as

$$V_{p,q} - V_{p,q}^{cap} - (R_{cap} + sL_{cap}) I_{p,q}^{cap} = 0$$
$$sC_{cap} V_{p,q}^{cap} - I_{p,q}^{cap} = 0 \tag{21}$$

where $V_{p,q}^{cap}$, $I_{p,q}^{cap}$ are the potential across the capacitance and current through the capacitance, respectively, while R_{cap}, L_{cap}, C_{cap} represent the series resistive, inductive, and capacitive contribution of the decoupling capacitor. Equation (21) can be incorporated in (12) and (20) to include the effect of decoupling capacitors.

D. Size of Unit Cell

The size of the unit cells directly affects the CPU run time costs as well as the accuracy of the model. The smaller the unit cell size, the better the accuracy of the model at the cost of larger circuit matrices in (17) and (20).

The transmission line segments of a discretized PDN structure (Fig. 2) are inherently improperly terminated at each node since each line segment is feeding a parallel combination of similar transmission lines; i.e., the load impedance seen by each transmission line segment is not equal to the characteristic impedance of the line segment. This mismatch in termination for each transmission line segment leads to multiple reflection of the transient waveform at every node [21]. To capture the effects of the reflection in the transient analysis, the maximum allowable length of the transmission line segments is limited to no more than one-fifth of a rise time for a transient waveform as suggested in [21]. This can be mathematically expressed as

$$l\sqrt{L_i C_i} \le \frac{T_r}{5} \tag{22}$$

where T_r is the rise time of the band limited excitation. This allows at least three reflections at the far end during the rise time of the excitation, whereby the energy of the reflected wave will have been attenuated considerably and not lead to transient simulation errors.

IV. Numerical Examples

Three examples are presented in this section to demonstrate the validity and efficiency of the proposed macromodel. The proposed model is implemented using MATLAB R2008a operating on DELL T7400 64-bit workstations with clock speed 3.16 GHz. The accuracy of the proposed algorithm was compared with the conventional lumped RLGC model [7],

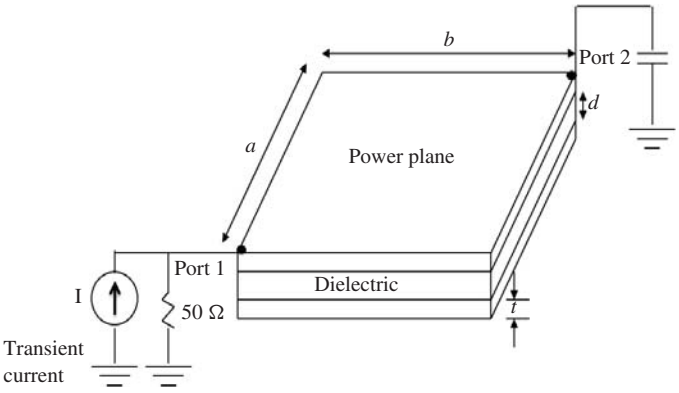

Fig. 3. Rectangular PDN structure of Example 1.

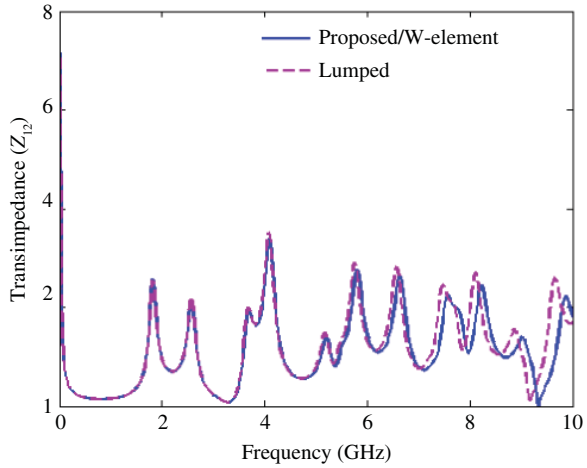

Fig. 4. Comparison of Z-parameters of Example 1 using proposed, W-element, and lumped models for transimpedance (Z_{12}).

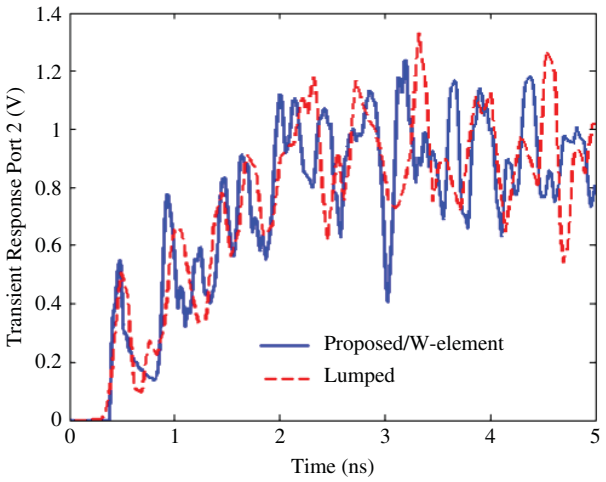

Fig. 5. Comparison of transient response at port 2 of Example 1 using proposed, W-element, and lumped model.

TABLE I
COMPARISON OF CPU RUN TIME OF PROPOSED MODEL WITH SPICE MODELS FOR EXAMPLE 1

Model	No. of unit cells (length of transmission line segment)	CPU time (s)	Mean difference w.r.t. W-element
Proposed	256 ($l = 0.25$ cm)	32.61	0.007
Lumped	256 ($l = 0.25$ cm)	158.10	0.152
	625 ($l = 0.16$ cm)	461.20	0.010
DEPACT-MNA	256 ($l = 0.25$ cm)	224.90	0.007

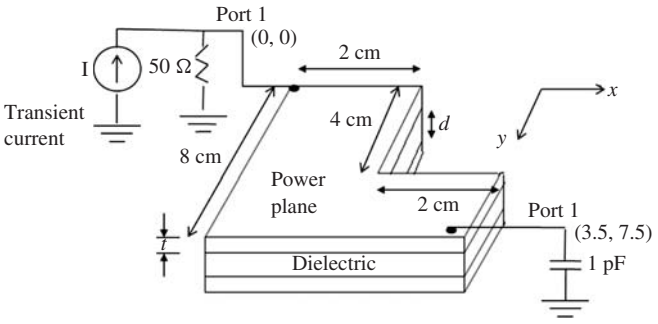

Fig. 6. L-shaped PDN of Example 2.

HSPICEs W-element model [21], and the DEPACT macromodel using MNA formulation (referred to as DEPACT-MNA) [34]–[36]. The CPU cost for the proposed model was compared with a customized version of the lumped RLGC model and DEPACT-MNA in MATLAB. It is noted that both lumped and DEPACT-MNA models require an *RL* ladder consisting of four sections to model the skin effect losses (i.e., $m = 4$). For the proposed model, a fourth-order rational approximation is sufficient when the error tolerance is 1×10^{-4} for a bandwidth of 10 GHz.

Example 1: The objective of the example is to illustrate the accuracy and efficiency achieved using the proposed model compared to existing SPICE models. A simple rectangular PDN of size 4 cm × 4 cm ($a = 4$ cm, $b = 4$ cm) as shown in Fig. 3 is considered. The signal and ground planes are made of copper of thickness $t = 30.5$ μm and separated by a $d = 25.4$ μm thick FR4 dielectric. The input is a current source that mimics the transient current induced during switching of the digital circuits. The PDN is loaded with a linear capacitor of 1 pF. Considering a source with rise time 0.1 ns, the size of the unit cell required for the proposed model using (22) is $l \leq 0.3$ cm and is set to 0.25 cm. Using the obtained cell dimensions in (2) and (3), the p.u.l. parameters of the transmission line segments are obtained, including skin effect losses.

Fig. 4 shows the Z-parameter of the transfer impedance (Z_{12}) of the PDN over a bandwidth of 10 MHz–10 GHz using (18) of the proposed model. In addition, the proposed algorithm is compared with the conventional lumped model and the W-element model of same discretization. It is found that the proposed model can accurately match the W-element model over the entire bandwidth, whereas the lumped model matches the W-element till 5 GHz.

To estimate the SSN, a trapezoidal input pulse of rise time 0.1 ns and pulse width of 2 ns is applied at port 1 while observing the transient response at port 2. Fig. 5 shows the

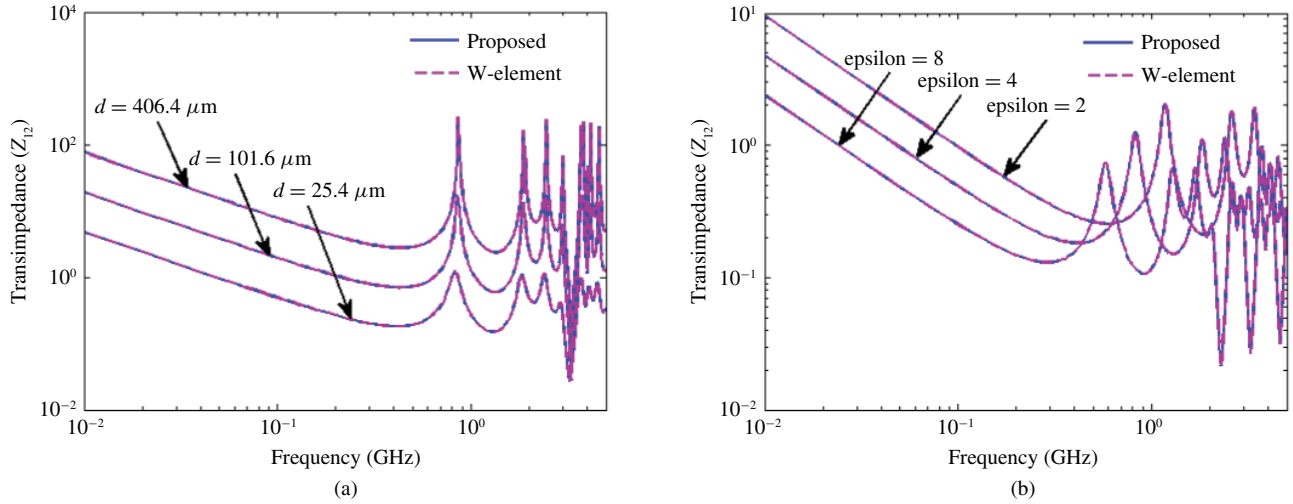

Fig. 7. Comparison of trans impedance (Z_{12}) of Example 2 for variation in dielectric thickness and relative permittivity using proposed and W-element models. (a) Variation in trans impedance (Z_{12}) with change in dielectric thickness. (b) Variation in trans impedance (Z_{12}) with change in relative permittivity.

transient response at port 2 obtained using (20) of the proposed model. In addition the proposed model is compared with the conventional lumped model and the W-element model for the same cell size. The proposed model yields similar responses as the W-element while the lumped model yields different responses.

Table I illustrates the computational expense and associated accuracy for the transient analysis using the proposed and existing SPICE models over 0–5 ns (Fig. 5). Note that the proposed and DEPACT-MNA models are about two orders of magnitude more accurate than the lumped model of same discretization. The accuracy of the lumped model can be improved by decreasing the cell size at the cost of increased CPU expense as shown in Table I. For this example, the proposed model provides an approximate speedup of 5 times over the lumped model and 7 times over the DEPACT-MNA model for $l = 0.25$ cm.

Example 2: The objective of this example is to illustrate the validity of the proposed model for a variety of dielectric materials and thicknesses. An L-shaped PDN shown in Fig. 6 is considered where the planes are made of copper of thickness of $t = 30.5$ μm and separated by a dielectric with varying thickness (d) and relative permittivity (ε_r). The input and output ports are located at (0, 0 cm) and (3.5 cm, 7.5 cm) as shown in Fig. 6. Considering a source with rise time 0.2 ns, the size of the unit cell obtained using (22) is $l \leq 0.6$ cm and set to 0.5 cm. Using the obtained cell dimensions in (2) and (3), the p.u.l. parameters of the transmission line segments are obtained including skin effect losses.

The L-shaped structure is first investigated for a variety of dielectric thicknesses (d), with the relative permittivity ε_r kept fixed at 4. Fig. 7(a) shows the Z-parameters of the PDN for $d = 25.4$ μm (1 mil), 101.6 μm (4 mil), and 406.4 μm (16 mil) using (18) of the proposed model. Next, the L-shaped structure is investigated for a variety of relative permittivity (ε_r) values while keeping the thickness constant at $d = 25.4$ μm. Fig. 7(b) shows the Z-parameters of the PDN for $\varepsilon_r = 2$, 4, and 8 using (18) of the proposed model. In either case, the proposed model is compared with the W-element model of same discretization and shows good agreement over the entire bandwidth.

From Fig. 7(a), it is observed that changing the dielectric thickness does not affect the resonant frequencies. This is because the speed of the transient wave through each transmission line segment is given by $\upsilon = l/\gamma = l/\sqrt{L_i C_i}$ which from (1) can be found to be independent of dielectric thickness [21]. However, increasing the dielectric thickness is found to significantly increase the impedance of the PDN [Fig. 7(a)] since the characteristic impedance of each transmission line segment, given by $Z_c = \sqrt{L_i/C_i}$, is linearly proportional to the dielectric thickness.

Increasing ε_r causes the capacitance of the PDN to increase and hence significantly decreases the low-frequency impedance [Fig. 7(b)]. However, the speed of the transient wave through each transmission line segment is proportional to $1/\sqrt{\varepsilon}$ [21]. Hence, increasing the relative permittivity shifts the resonant frequencies from the high-frequency region to the low-frequency region [Fig. 7(b)].

To mimic the SSN propagation over the PDN, a trapezoidal input waveform of unit amplitude, rise time 0.2 ns, pulse width 0.2 ns, and time period 1.2 ns is applied at port 1 and the transient waveform at port 2 is observed. Note that the frequency of the input waveform corresponds to the first resonance frequency of 830 MHz [Fig. 7(a)]. Fig. 8 shows the transient responses at port 2 with dielectric thickness $d = 25.4$ μm and 101.6 μm [$\varepsilon_r = 4$ same as in Fig. 7(a)] obtained using (20) and is compared with the W-element. Since the resonance frequencies of both structures of Fig. 8 remain unchanged with variation in dielectric thickness, both structures yield a resonating transient signature when excited by the above source. However, due to the increase of the impedance of the structure with increase in dielectric thickness, the steady-state noise amplitude at port 2 is increased by 4.3 times as the dielectric thickness is increased from $d = 25.4$ μm to $d = 101.6$ μm. Fig. 9 shows the far-

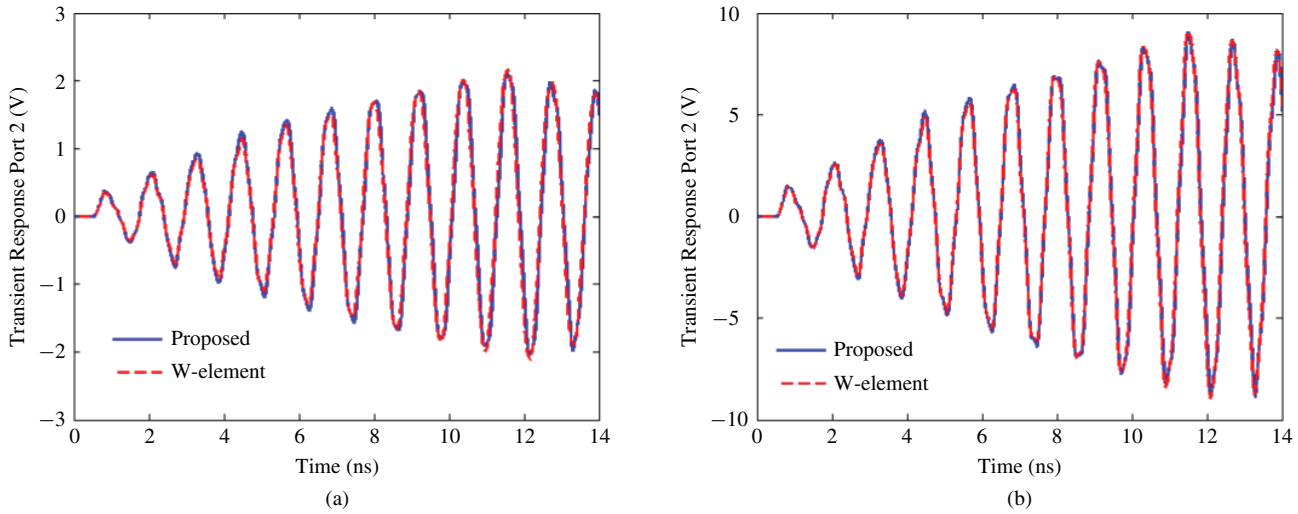

Fig. 8. Comparison of transient response of Example 2 with variation in dielectric thickness using proposed and W-element models. Relative permittivity fixed at 4. (a) Dielectric thickness $d = 25.4$ μm. (b) Dielectric thickness $d = 101.6$ μm.

TABLE II
COMPARISON OF CPU RUN TIME OF PROPOSED MODEL WITH SPICE MODELS FOR EXAMPLE 2

Model	No. of unit cells (length of transmission line segment)	CPU time (s)	Mean difference w.r.t. W-element
Proposed	96 ($l = 0.5$ cm)	10.05	0.002
Lumped	96 ($l = 0.5$ cm)	48.80	0.040
	216 ($l = 0.33$ cm)	129.50	0.008
DEPACT-MNA	96 ($l = 0.5$ cm)	69.40	0.003

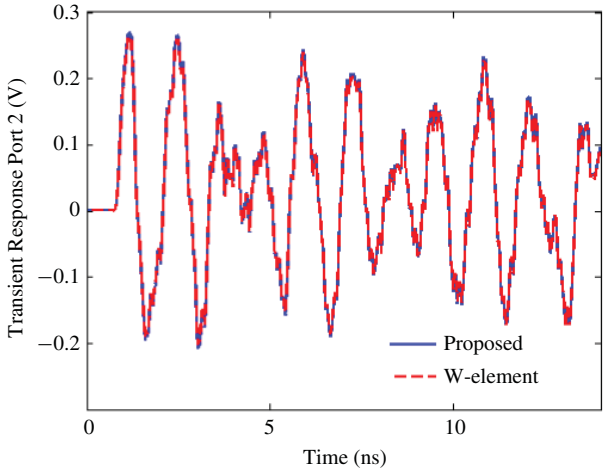

Fig. 9. Comparison of transient response of Example 2 using proposed and W-element models. Dielectric thickness $d = 25.4$ μm and relative permittivity is 2.

end transient responses of the PDN with relative permittivity changed to $\varepsilon_r = 2$ ($d = 25.4$ μm) and excited by the same source. Since changing the relative permittivity causes a shift in the resonance frequencies [Fig. 7(b)], the transient response of Fig. 9 no longer shows the resonance characteristics as illustrated in Fig. 8 despite using the same input source.

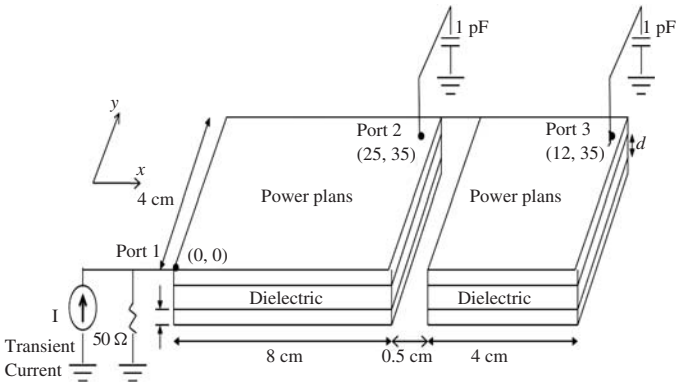

Fig. 10. PDN structure of Example 3.

Table II illustrates the computational expense for transient simulations of Figs. 8 and 9 using the proposed and existing SPICE models over 0–12 ns. Note that the proposed and DEPACT-MNA model are about one order of magnitude more accurate than the lumped model of same discretization. For this example, the proposed model provides an approximate speedup of 5 times over the lumped model for $l = 0.5$ cm, 13 times over the lumped model for $l = 0.33$ cm, and 7 times over the DEPACT-MNA model ($l = 0.5$ cm).

Example 3: This example seeks to model the effect of decoupling capacitors on the peak SSN noise. For this example, a split plane as depicted in Fig. 10 is considered. The PDN consisted of two rectangular planes of 8 cm $\times$ 4 cm and 4 cm $\times$ 4 cm, coupled together using a ferrite core, which is represented as a parallel combination of $R = 25$ Ω, $C = 0.15$ pF, and $L = 0.17$ nH as suggested in [7]. The planes are made of copper of thickness of $t = 30.5$ μm and separated by a $d = 25.4$ μm thick FR4 dielectric. The input port (port 1) is located at (0, 0) and the output ports (port 2 and 3) are located at (7.5 cm, 3.5 cm, and 12 cm), respectively (Fig. 10). Considering a source with rise time 0.2 ns, the size of the unit cell required obtained using (22) is $l \leq 0.6$ cm and set

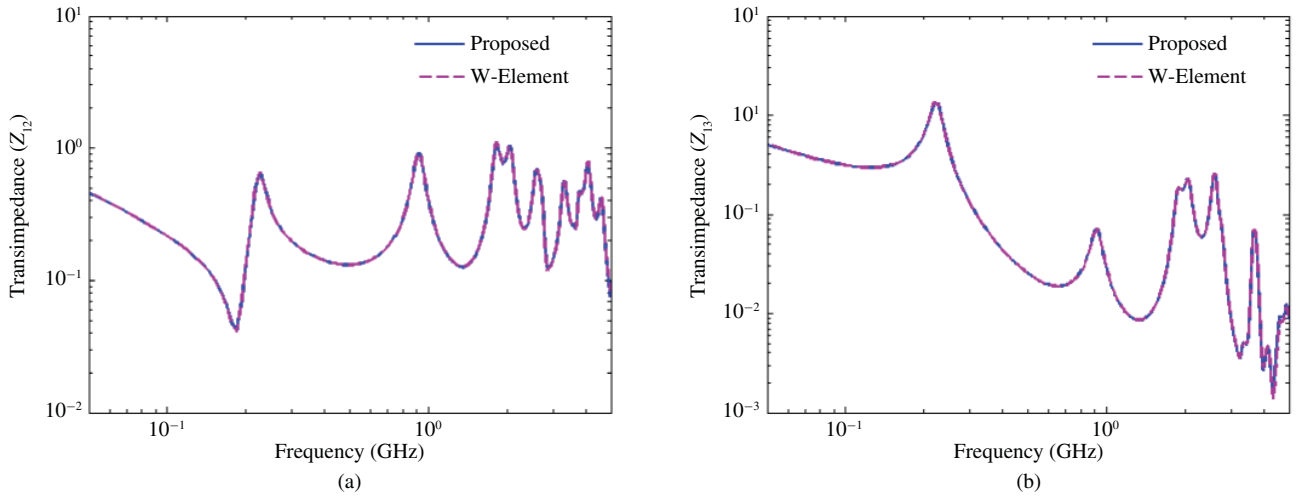

Fig. 11. Comparison of Z-parameters of Example 3 using proposed and W-element models. (a) Transimpedance (Z_{12}). (b) Transimpedance (Z_{13}).

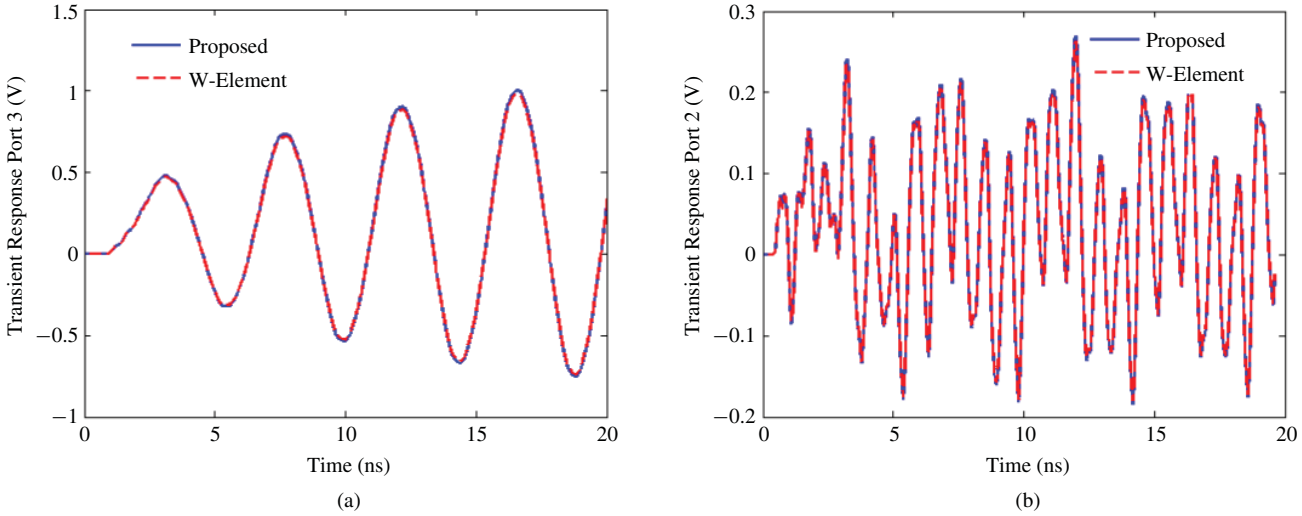

Fig. 12. Effect of decoupling capacitors on transient response of Example 3 using proposed and W-element models. (a) Transient response at port 3 without decoupling capacitors. (b) Transient response at port 3 including decoupling capacitors.

to 0.5 cm. Using the obtained cell dimensions in (2) and (3), the p.u.l. parameters of the transmission line segments are obtained including skin effect losses. Initially, decoupling capacitors are assumed absent and the Z-parameters of the three-port network are evaluated using (18) of the proposed model and compared with the W-element model of the same discretization as shown in Fig. 11.

To simulate the effect of SSN, a trapezoidal input waveform of unit amplitude, rise time 0.2 ns, pulse width 1.8 ns, and time period 4.4 ns is applied at port 1 and the transient waveform at port 2 and 3 is observed. Note that the frequency of the input waveform corresponds to the first resonance frequency (225 MHz) of the PDN (Fig. 11). Fig. 12(a) shows the resonance at the output ports 3 obtained using (20). To observe the effect of decoupling capacitors on the peak noise signal, decoupling capacitors modeled by a series *RLC* model of $R_d = 0.1\ \Omega$, $R_d = 0.1\ \Omega$, $L_d = 2$ nH, $C_d = 100$ pF $L_d = 2nH$, and $C_d = 100$ pF are placed at the nodes of the discretized PDN. To observe the effect of the decoupling capacitors on the SSN, the PDN is again excited by the same source and the transient response of port 3 is evaluated using (20) in Fig. 12(b). It is observed that inclusion of the decoupling capacitors prevents the resonance characteristics from occurring and damps the amplitude of the noise signal.

TABLE III
COMPARISON OF CPU RUN TIME OF PROPOSED MODEL WITH SPICE MODELS FOR EXAMPLE 3

Model	No. of unit cells (length of transmission line segment)	CPU time (s)	Mean difference w.r.t. W-element
Proposed	192 ($l = 0.5$ cm)	20.75	0.004
Lumped	192 ($l = 0.5$ cm)	120.00	0.027
	432 ($l = 0.33$ cm)	298.70	0.009
DEPACT-MNA	192 ($l = 0.5$ cm)	180.40	0.003

Table III illustrates the computational expense or transient simulations of Fig. 12 using the proposed and existing SPICE

models over 0–20 ns. Note that the proposed and DEPACT-MNA model are about one order of magnitude more accurate than the lumped model of same discretization. For this example, the proposed model provides an approximate speedup of 6 times over the lumped model for $l = 0.5$ cm, 15 times over the lumped model for $l = 0.33$ cm, and 9 times over the DEPACT-MNA model ($l = 0.5$ cm).

V. Conclusion

In this paper, an efficient broadband approach for analysis of irregular shaped PDN was proposed. The proposed methodology is based on discretization of the plane into an orthogonal grid of transmission line segments. Using a delay extraction based model for each line segments, a compact model was achieved where the size of the circuit matrices depends only on the size of the orthogonal grid while all other variables due to the transmission line macromodel are eliminated. This approach of eliminating extra variables was extended to include skin effect losses without augmentation of the circuit matrices. Numerical examples showed significant savings in memory and run time costs by the proposed model compared to the existing SPICE macromodels for a variety of structures, geometries, and materials.

References

[1] E. E. Davidson, "Electrical design of a high speed computer package," *IBM J. Res. Develop.*, vol. 26, no. 3, pp. 349–361, May 1982.

[2] R. R. Tummala, E. J. Rymaszewski, and A. G. Klopfenstein, *Microelectronics Packaging Handbook, Part I*, 2nd ed. London, U.K.: Chapman & Hall, 1997.

[3] B. Young, *Digital Signal Integrity*. Englewood Cliffs, NJ: Prentice-Hall, 2001, ch. 11.

[4] I. Novak, "Reducing simultaneous switching noise and EMI on ground/power planes by dissipative edge termination," *IEEE Trans. Adv. Packag.*, vol. 22, no. 3, pp. 274–283, Aug. 1999.

[5] I. Novak, "Lossy power distribution networks with thin dielectric layers and/or thin conductive layers," *IEEE Trans. Adv. Packag.*, vol. 23, no. 3, pp. 353–360, Aug. 2000.

[6] K. Lee and A. Barber, "Modeling and analysis of multichip module power supply planes," *IEEE Trans. Compon. Packag. Manuf. Tech.*, vol. 18, no. 4, pp. 628–639, Nov. 1995.

[7] J.-H. Kim and M. Swaminathan, "Modeling of irregular shaped power distribution planes using transmission matrix method," *IEEE Trans. Adv. Packag.*, vol. 24, no. 3, pp. 334–346, Aug. 2001.

[8] R. Achar, M. S. Nakhla, H. S. Dhindsa, A. R. Sridhar, D. Paul, and N. M. Nakhla, "Parallel and scalable transient simulator for power grids via waveform relaxation (PTS-PWR)," *IEEE Trans. Very Large Scale Integr. Syst.*, vol. 19, no. 2, pp. 319–332, Feb. 2011.

[9] S. Berghe, F. Olyslager, D. de Zutter, J. de Moerloose, and W. Temmerman, "Study of the ground bounce caused by power plane resonances," *IEEE Trans. Electromagn. Compat.*, vol. 40, no. 2, pp. 111–119, May 1998.

[10] R. Mitra, S. Chebolu, and W. D. Becker, "Efficient modeling of power planes in computer packages using the finite difference time domain method," *IEEE Trans. Microw. Theory Tech.*, vol. 42, no. 9, pp. 1791–1795, Sep. 1994.

[11] T. K. Sarkar, B. Kolundjiza, A. R. Djordjevic, and M. Salazar-Palma, "Accurate modeling of frequency responses of multiple planes in gigahertz packages and boards," in *Proc. 9th IEEE Conf. Electr. Perform. Electron. Packag.*, Scottsdale, AZ, Oct. 2000, pp. 59–62.

[12] C. Guo and T. H. Hubing, "Circuit models for power bus structures on printed circuit boards using a hybrid FEM-SPICE method," *IEEE Trans. Adv. Packag.*, vol. 29, no. 3, pp. 441–447, Aug. 2006.

[13] B. Archambeault and A. E. Ruehli, "Analysis of power/ground-plane EMI decoupling performance using the partial-element equivalent circuit technique," *IEEE Trans. Electromagn. Compat.*, vol. 43, no. 4, pp. 437–445, Nov. 2001.

[14] J. Choi, S.-H. Min, J.-H. Kim, M. Swaminathan, W. Beyene, and X. Yuan, "Modeling and analysis of power distribution networks for Gigabit applications," *IEEE Trans. Mobile Comput.*, vol. 2, no. 4, pp. 299–313, Oct.–Dec. 2003.

[15] N. Na, J. Choi, S. Chun, and M. Swaminathan, "Modeling and transient simulation of planes in electronic packages," *IEEE Trans. Adv. Packag.*, vol. 23, no. 3, pp. 340–352, Aug. 2000.

[16] M. A. Schmitt, K. Lam, L. E. Mosley, G. Choksi, and B. K. Bhattacharyya, "Current distribution in power and ground planes of a multilayer pin grid packages," in *Proc. Int. Electron. Packag. Soc.*, 1988, pp. 467–475.

[17] W. Becker, B. McCredie, G. Wilkins, and A. Iqbal, "Power distribution modelling of high performance first level computer packages," in *Proc. IEEE 2nd Electr. Perform. Electron. Packag.*, Monterey, CA, Oct. 1993, pp. 202–205.

[18] H. Kubota, A. Kamo, T. Watanabe, and H. Asai, "Analysis of power/ground planes by PCB simulator with model order reduction technique," in *Proc. 10th Electr. Perform. Electron. Packag.*, Cambridge, MA, Oct. 2001, pp. 77–80.

[19] T. Watanabe and H. Asai, "Model order reduction of electromagnetic systems and RLC circuits for power plane resonance analysis," in *Proc. 12th Electr. Perform. Electron. Packag.*, Oct. 2003, pp. 203–206.

[20] H. H. Wu, J. W. Meyer, K. Lee, and A. Barber, "Accurate power supply and ground plane pair models," *IEEE Trans. Adv. Packag.*, vol. 22, no. 3, pp. 259–266, Aug. 1999.

[21] L. Smith, R. Raymond, and T. Roy, "Power plane SPICE models and simulated performance for materials and geometries," *IEEE Trans. Adv. Packag.*, vol. 24, no. 3, pp. 277–287, Aug. 2001.

[22] N. Nakhla, A. E. Ruehli, M. Nakhla, R. Achar, and C. Chen, "Waveform relaxation techniques for simulation of coupled interconnects with frequency-dependent parameters," *IEEE Trans. Adv. Packag.*, vol. 30, no. 2, pp. 257–269, May 2007.

[23] *HSPICE Signal Integrity User Guide*, Synopsys Inc., Mountain View, CA, Sep. 2009.

[24] F. H. Branin, Jr., "Transient analysis of lossless transmission lines," *Proc. IEEE*, vol. 55, no. 11, pp. 2012–2013, Nov. 1967.

[25] F.-Y. Chang, "The generalized method of characteristics for waveform relaxation analysis of lossy coupled transmission lines," *IEEE Trans. Microw. Theory Tech.*, vol. 37, no. 12, pp. 2028–2038, Dec. 1989.

[26] S. Grivet-Talocia, H.-M. Huang, A. E. Ruehli, F. Canavero, and I. M. Elfadel, "Transient analysis of lossy transmission lines: An efficient approach based on the method of characteristics," *IEEE Trans. Adv. Packag.*, vol. 27, no. 1, pp. 45–56, Feb. 2004.

[27] A. Dounavis and V. A. Pothiwala, "Passive closed-form transmission line macromodel using method of characteristics," *IEEE Trans. Adv. Packag.*, vol. 31, no. 1, pp. 190–202, Feb. 2008.

[28] A. Dounavis, V. A. Pothiwala, and A. Beygi, "Passive macromodeling of lossy multiconductor transmission lines based on the method of characteristics," *IEEE Trans. Adv. Packag.*, vol. 32, no. 1, pp. 184–198, Feb. 2009.

[29] I. M. Elfadel, H.-M. Huang, A. E. Ruehli, A. Dounavis, and M. S. Nakhla, "A comparative study of two transient analysis algorithms for lossy transmission lines with frequency-dependent data," *IEEE Trans. Adv. Packag.*, vol. 25, no. 2, pp. 143–153, May 2002.

[30] A. Dounavis, R. Achar, and M. Nakhla, "Efficient passive circuit models for distributed networks with frequency-dependent parameters," *IEEE Trans. Adv. Packag.*, vol. 23, no. 8, pp. 382–392, Aug. 2000.

[31] A. Dounavis, R. Achar, and M. Nakhla, "A general class of passive macromodels for lossy multiconductor transmission lines," *IEEE Trans. Microw. Theory Tech.*, vol. 49, no. 10, pp. 1686–1696, Oct. 2001.

[32] A. Cangellaris, S. Pasha, J. L. Prince, and M. Celik, "A new discrete transmission line model for passive model order reduction and macromodeling of high-speed interconnections," *IEEE Trans. Adv. Packag.*, vol. 22, no. 3, pp. 356–364, Aug. 1999.

[33] Q. Yu, J. M. L. Wang, and E. S. Kuh, "Passive multipoint moment matching model order reduction algorithm on multiport distributed interconnect networks," *IEEE Trans. Circuits Syst. I: Fundam. Theory Appl.*, vol. 46, no. 1, pp. 140–160, Jan. 1999.

[34] S. Roy and A. Dounavis, "Efficient macromodeling of power distribution planes using delay extraction based transmission line representation," in *Proc. 14th Int. Symp. Antenna Technol. Appl. Electromagn. Amer. Electromagn. Conf.*, Ottawa, ON, Jul. 2010, pp. 1–4.

[35] N. M. Nakhla, A. Dounavis, R. Achar, and M. S. Nakhla, "DEPACT: Delay extraction-based passive compact transmission-line macromodeling algorithm," *IEEE Trans. Adv. Packag.*, vol. 28, no. 1, pp. 13–23, Feb. 2005.

[36] N. Nakhla, M. S. Nakhla, and R. Achar, "Simplified delay extraction-based passive transmission line macromodeling algorithm," *IEEE Trans. Adv. Packag.*, vol. 33, no. 2, pp. 498–509, May 2010.
[37] C. R. Paul, *Analysis of Multiconductor Transmission Line*. New York: Wiley, 2008.
[38] K. S. Oh, "Accurate transient simulation of transmission lines with the skin effect," *IEEE Trans. Comput.-Aid. Des. Integr. Circuits Syst.*, vol. 19, no. 3, pp. 389–396, Mar. 2000.
[39] A. Odabasioglu, M. Celik, and L. T. Pilleggi, "PRIMA: Passive reduced-order interconnect macromodeling algorithm," *IEEE Trans. Comput.-Aid. Des. Integr. Circuits Syst.*, vol. 17, no. 8, pp. 645–653, Aug. 1998.
[40] S. Lin and E. S. Kuh, "Transient simulation of lossy interconnects based on the recursive convolution formulation," *IEEE Trans. Circuits Syst. I: Fundam. Theory Appl.*, vol. 39, no. 11, pp. 879–892, Nov. 1992.
[41] S. N. Lalgudi, E. Engin, G. Casinovi, and M. Swaminathan, "Accurate transient simulation of interconnects characterized by band-limited data with propagation delay enforcement in a modified nodal analysis framework," *IEEE Trans. Eletromagn. Compat.*, vol. 50, no. 3, pp. 715–729, Aug. 2008.

Sourajeet Roy (S'11) received the B.Tech. degree in electrical engineering from Sikkim Manipal University, Kolkata, India, in 2006, and the M.E.Sc. degree from the University of Western Ontario, London, ON, Canada, in 2009. He is currently pursuing the Ph.D. degree at the Department of Electrical and Computer Engineering, University of Western Ontario.

His current research interests include numerical algorithms for efficient transient simulation of high-speed packages.

Mr. Roy was the recipient of the Vice-Chancellor's Gold Medal for academic excellence at the undergraduate level.

Anestis Dounavis (S'00–M'03) received the B.E. degree in electrical engineering from McGill University, Montreal, QC, Canada, in 1995, and the M.Sc. and Ph.D. degrees in electrical engineering from Carleton University, Ottawa, ON, Canada, in 2000 and 2004, respectively.

He is currently working as an Associate Professor in the Department of Computer and Electrical Engineering, University of Western Ontario, London, ON. His current research interests include electronic design automation, simulation of high-speed and microwave networks, signal integrity, and numerical algorithms.

Dr. Dounavis was the recipient of the Ottawa Centre for Research and Innovation Futures Award, Student Researcher of the Year in 2004, and the INTEL Best Student Paper Award at the Electrical Performance of Electronic Packaging Conference in 2003. He received the Carleton University Medal for outstanding graduate work at the M.Sc. and Ph.D. levels in 2000 and 2004, respectively. He was the recipient of the University Student Council Teaching Honour Roll Award at the University of Western Ontario from 2009 to 2010.